



# Earthquake rupture dependence on hypocentral location along the Nicoya Peninsula subduction megathrust

Hongfeng Yang<sup>a,\*</sup>, Suli Yao<sup>a</sup>, Bing He<sup>a</sup>, Andrew V. Newman<sup>b</sup>

<sup>a</sup> Earth System Science Programme, The Chinese University of Hong Kong, Shatin, Hong Kong, China

<sup>b</sup> School of Earth and Atmospheric Sciences, Georgia Institute of Technology, Atlanta, GA, USA

## ARTICLE INFO

### Article history:

Received 19 November 2018

Received in revised form 13 May 2019

Accepted 19 May 2019

Available online 31 May 2019

Editor: M. Ishii

### Keywords:

interseismic locking

spontaneous rupture simulation

hypocentre-dependent earthquake

magnitude

near-field tsunami early warning

## ABSTRACT

Although interseismic locking distributions have been used in qualitatively evaluating the future earthquake potential, quantitatively estimating how an earthquake may rupture through the locked interface is a more useful tool for quantifying both seismic and tsunami hazards. Here, we investigate rupture scenarios from interseismic locking models along the megathrust interface below Nicoya Peninsula, Costa Rica using spontaneous rupture simulations. We first estimate initial stress from locking, then initiate spontaneous ruptures at different nucleation points and observe the eventual earthquake magnitudes and slip distribution. We find that ~40% of nucleations tested develop into large earthquakes of  $M_w > 7.2$  based on present interseismic locking models. Of these events, those nucleated from deeper depths have a tendency for larger-amplitude shallow slip, suggesting increased tsunami potential. Furthermore, irrespective of the input locking models we do not observe rupture scenarios of earthquakes with intermediate magnitudes between 6 and 7, a result consistent with observations in Nicoya. The results of hypocentre-dependent earthquake magnitudes and tsunamigenic potential not only pose challenges in estimating rupture extents from locking models, but also underscore the significance of quantitatively evaluating seismic and tsunami hazard in subduction zones.

© 2019 Elsevier B.V. All rights reserved.

## 1. Introduction

In past decade, interseismic locking distribution derived from geodetic studies has significantly improved our understanding of a future earthquake's potential, in particular at subduction zones where great earthquakes occur, sometimes causing devastating tsunamis (e.g. Moreno et al., 2010; Wang et al., 2012; McCaffrey et al., 2013). However, considerable uncertainties exist in such interseismic locking models depending on different material rheology properties, subduction fault geometry, and dataset that are used to constrain the locking. One fundamental limit comes from the fact that the locked-then-ruptured megathrust interface resides almost exclusively offshore in subduction zone environments, with limited constraints from inland observations. A typical example is the Cascadia subduction zone where dense on-land geodetic networks are available. Although it is believed the Cascadia megathrust is locked, the present locking models show considerable controversies in the locking degree and downdip spatial extent along Central

Oregon (Burgette et al., 2009; McCaffrey et al., 2013; Schmalzle et al., 2014; Pollitz and Evans, 2017; Li et al., 2018). Even for a subduction environment such as the Nicoya Peninsula of Costa Rica, where the locked-then-ruptured patch is almost entirely located under land, different locking models have been obtained using different datasets and megathrust geometry (Feng et al., 2012; Xue et al., 2015; Kyriakopoulos and Newman, 2016). Thus, it remains unclear how to infer future earthquake sizes from the locking models.

Quantitative evaluations of future rupture scenarios from interseismic locking distributions were performed in a few subduction zones. For instance, Hok et al. (2011) developed dynamic rupture scenarios of anticipated Nankai-Tonankai earthquakes, southwest Japan using a boundary integral method. They concluded that rupture segmentation was associated with the prescribed along-strike variation of fracture energy. Because we do not know when the next Nankai-Tonankai earthquake will occur, we cannot yet compare the numerical rupture scenarios with field observations recorded by modern instruments. More recently, Yang et al. (2019) derived rupture scenarios from locking models in the Nicoya Peninsula, Central America, and then validated the numerical results with kinematic source models of the 2012  $M_w$  7.6

\* Corresponding author.

E-mail address: [hyang@cuhk.edu.hk](mailto:hyang@cuhk.edu.hk) (H. Yang).

Nicoya earthquake, which occurred directly under the peninsula. The rupture was initiated at the hypocentre of the 2012 Nicoya earthquake and spontaneously propagated on the fault plane (Yang et al., 2019). The final moment magnitude, coseismic slip distribution, and moment rate function are well consistent with those kinematic solutions (Yue et al., 2013), demonstrating that, for the first time, deriving a reasonable approximation of the coseismic slip distribution and rupture process from interseismic locking is feasible (Yang et al., 2019).

Although it seems possible to derive reliable rupture scenarios (Yang et al., 2019), it is critical that such a model also accurately describes rupture nucleation from the hypocentre of the 2012 Nicoya earthquake. Indeed, we do not know where future earthquakes may nucleate (Lapusta and Rice, 2003; Hori et al., 2004), owing to our limited understanding of loading and the heterogeneous distribution of stress and fault strength. Even after the occurrence of an earthquake, e.g. the 2012 Nicoya earthquake, hypocentre bears uncertainties depending on data used and method of determination (Quintero et al., 2014; Yue et al., 2013). For example, the hypocentre used to derive kinematic source process in Yue et al. (2013) corresponds to a low stress environment in both locking models (Feng et al., 2012; Xue et al., 2015). Because we do not know where future earthquakes may nucleate solely based on locking models, we investigate the effects of nucleation positions on coseismic rupture scenarios.

In this study, we conduct spontaneous rupture simulations based on interseismic locking models by considering a range of hypocentral locations. Our geographical focus is the Nicoya Peninsula because it protrudes seaward, forming a unique environment allowing near-field inland geodetic observations directly above one of the locked patches (Fig. 1). As such, the locking models in the region bear much less uncertainties than those in other subduction zones. We will derive hypocentral dependent rupture scenarios from two late-interseismic locking models that were derived along the same curvilinear megathrust geometry, one building on trench-normal and vertical GPS from 1996 to 2010 (Feng et al., 2012) while the other one also incorporating trench-parallel GPS and line-of-sight Interferometric Synthetic Aperture Radar (InSAR) data from 2007 to 2011 that may have improved some resolution of features (Xue et al., 2015). Even with the most precise and dense land-based geodetic data, offshore resolvability of megathrust interface features drop-off rapidly, and the ability to recover substantial locking or slip information more than 20 km offshore is negligible (Williamson and Newman, 2018). Fore-knowledge of such limitations was one of the reasons that Nicoya was chosen for continued study, because the location of the peninsula places the locking and seismogenic slip region directly under land, and available for detailed analysis.

## 2. Method and model set up

Here we conduct spontaneous rupture simulations using a finite element package, Pylith (Aagaard et al., 2013). A number of ingredients to simulating dynamic ruptures play critical roles in the results, including fault geometry and material properties, as well as appropriately estimating the initial stress distribution and constitutive parameters. A smoothly curved fault geometry that was used to invert for the locking models (Feng et al., 2012; Xue et al., 2015) is used to generate the mesh. The fault model created by Feng and later used by Xue was created from a central 2D transect of 3D relocated microseismicity within the central Nicoya Peninsula (see Feng et al., 2012), corresponding to the central locked region. This model remains a good approximation for the northern portion of Nicoya, however southern Nicoya does have a higher-standing plateau as later clearly observed in Kyriakopoulos et al. (2015). As shown in Yang et al. (2019), rupture scenarios in

the Nicoya region appear to be independent on material properties. Therefore, we incorporate a half space material property in our domain, which extends 180 km along-strike, 170 km perpendicular to strike, and 80 km at depth. All boundaries except for the free surface are set as absorbing boundaries to avoid energy reflected from the boundary surfaces.

The fault is governed by the linear slip-weakening law (Ida, 1972). Effective normal stress,  $\bar{\sigma} = \sigma - p$ , is the difference between normal stress  $\sigma$  and pore-pressure  $p$ . The pore-pressure in subduction zones is suggested to be close to lithostatic at the up-dip and down-dip ends of the seismogenic zone (Saffer and Tobin, 2011). Therefore, effective normal stress can be approximated by a constant as discussed by Rice (1992). For simplicity, the effective normal stress is taken as 50 MPa, as is commonly used in previous studies (e.g., Yang et al., 2012; Weng and Yang, 2017). The critical slip distance is taken as a spatially uniform constant, 0.4 m, consistent with the average value of the 2012 Nicoya earthquake that was estimated from near-field observations (Yao and Yang, 2018).

To estimate the initial stress distribution, it is critical to create a sufficiently good slip deficit and rupture history approximation. Here, we follow the approach adopted in Yang et al. (2019). Our primary limitation is that we assume that immediately after the prior earthquake, the fault locks up, and that the features we saw in the late interseismic are the same as they were just after the last event. With this assumption, the slip deficit can be summed as the linear accumulation of stress build-up between events. This assumption is reasonable in the Nicoya region, because nearly no interface earthquakes with magnitudes larger than 6 occurred in the locked region between the more characteristic  $M_w$  7.5+ megathrust events (Fig. 1). Thrust earthquakes with moment magnitudes larger than 5 are also limited according to the GCMT catalogue (Fig. 1), indicating very little seismic release of the slip deficit on the megathrust. Moreover, detected slow slip events (SSEs) in the region have very small spatial overlaps with the locked patches (Dixon et al., 2014). If the overlapped region did slip in slow slip events before the 2012  $M_w$  7.6 earthquake, our slip deficit will be slightly overestimated because SSEs usually slip in centimetres in an individual event. Thus, the potential effects of SSEs on slip deficit in the locking regions are minimal and would not significantly affect our results. Furthermore, we test potential impact of uncertainties in slip deficit on our rupture scenarios by considering a plate convergence rate of 11 mm/yr higher than the suggested value (82 mm/yr). The moment magnitudes and final slip distribution derived from both locking models are not significantly affected (Fig. S1), reassuring that uncertainties in the amplitude of the slip deficit play little roles in our results.

We next assume that the accumulated slip deficit will be completely released by a large ( $M > 7$ ) earthquake because we aim at evaluating the worst scenario. Thus the slip deficit is used to calculate the static stress drop of the earthquake. Since the last  $M_w$  7.5+ 1950 earthquake, the stress build-up  $\Delta\tau$  is calculated from the slip deficit for 62 yr (1950–2012). The initial stress  $\tau_0$  is then calculated from the stress drop and a constant dynamic friction coefficient (Weng and Yang, 2018; Yang et al., 2019), showing a heterogeneous distribution corresponding to the locking models (Fig. 2a and d). High stress regions generally correlate with patches of high locking degrees ( $>0.75$ ) because the variation in locking degrees is rather smooth in the two locking models. However, the highest stress regions appear to locate near the edge of the down-dip locked patch (Fig. 2a and d), where the locking gradient is the largest. Fault strength  $\tau_s$  is assumed to be spatially uniform and is set to be slightly larger than the maximum initial stress (Yang et al., 2019). Because the locking models are regularized by smoothing parameters, generally that minimize the second-order derivative of slip (first-order derivative of strain or stress), and a selective choice is made that will control the resultant fault stress

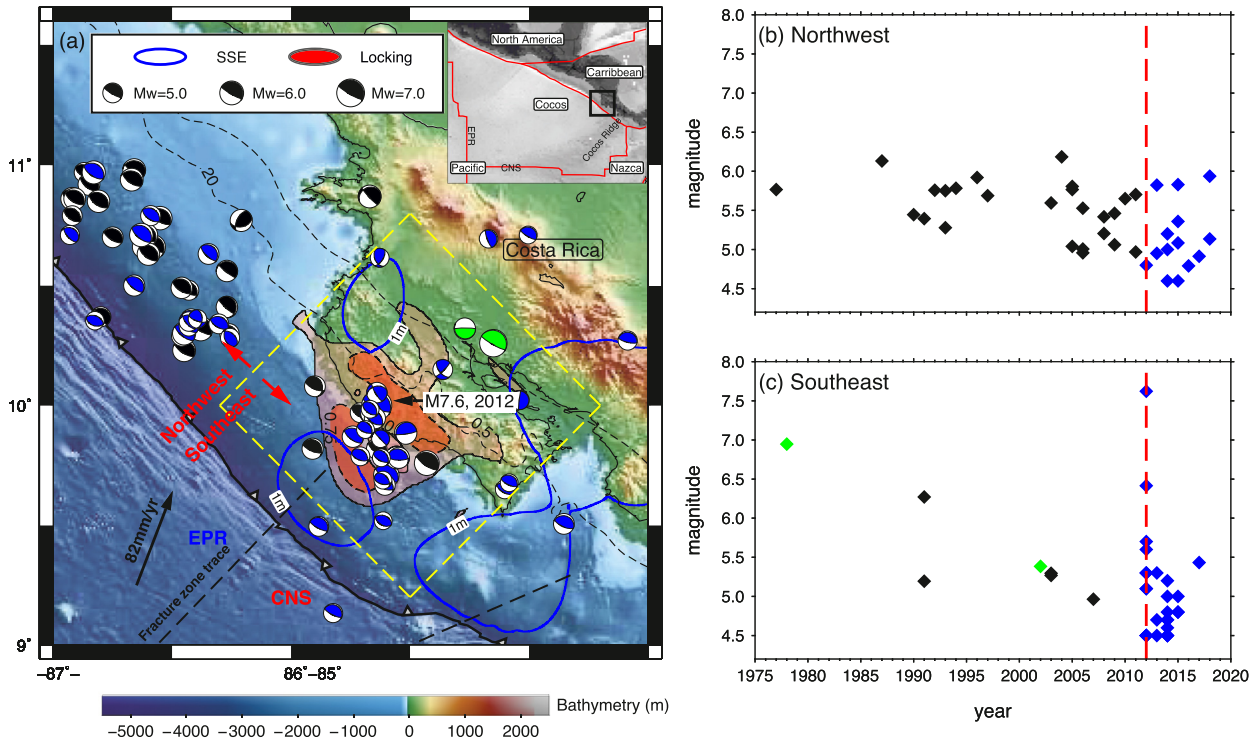


**Fig. 1.** (a) (inset) Tectonic setting of the Nicoya Peninsula. The interseismic locking contours (locking degrees of 0.75 and 0.5) and moment tensor solutions of interface earthquakes in the region. Colours of beach balls show occurrence time before (black: GCMT) and after (blue: GCMT and Chaves et al., 2017) the 2012 mainshock, as well as inland locations (green). Areas with slow slip events are shown in blue polygons, which represent 1 m of accumulative slip. Thin dashed lines show slab top depth contours of 20 and 40 km (Kyriakopoulos et al., 2015), respectively, EPR: East Pacific Rise; CNS: Cocos-Nazca spreading centre. (b) Magnitude and occurrence time of interface earthquakes northwest to (b) and beneath the peninsula (c). Colours correspond to the beach balls in panel (a). (For interpretation of the colours in the figure(s), the reader is referred to the web version of this article.)

field, the fields derived here should be considered in a relative sense.

### 3. Effect of nucleation zone locations on coseismic ruptures

Given the heterogeneous stress distribution, the rupture is expected to nucleate from the high stress regions subject to tectonic loading at greater depths. However, the SSEs surrounding the locked patches may potentially promote coseismic ruptures initiating from the shallow region (Fig. 1). Indeed, seven SSEs were identified in the Nicoya region from April 2007 to April 2012, with irregular intervals (4–16 months) and summed slip comparable to that of the 2012 Nicoya earthquake but in a much more expanded area (Dixon et al., 2014). Furthermore, although it is not quantified, heterogeneous strength distribution on the megathrust is implied by seismic studies (Audet and Schwartz, 2013; Chaves and Schwartz, 2016), and thus the rupture may start from any location in the locking region. Therefore, we divide the locking region into an 8 by 9 grid and nucleate the rupture in each node (Fig. 3a) to observe the eventual rupture scenarios.

Since we focus on the coseismic process, we artificially nucleate ruptures in a circular patch by decreasing the strength 0.01 MPa lower than the average initial stress to avoid non-uniform stress excess at different locations. We also ensure a reasonable rupture speed ( $<0.8$  Vs) within the nucleation zone to minimize the artificial nucleation effects (Bizzarri, 2010). It has been discussed in details how the sizes of nucleation zones vary in different locations given a heterogeneous stress distribution (Ripperger et al., 2007; Yang et al., 2019). Here we adopt a few circular radii (i.e. 3, 4, and 5 km) as the nucleation sizes. We consider 5 km as our upper limit because it corresponds to the typical rupture dimension of an M6 earthquake ( $\sim 10$  km). Consequently, rupture scenarios with mag-

nitudes less than 5 should be ignored because of our lower limit on the nucleation size.

The resultant 216 rupture scenarios are dependent on the location of nucleation within the grid due to the heterogeneous stress distribution. Even for two ruptures that started in neighbouring locations at the same depth with nearly identical initial stress level, the eventual slip distributions and earthquake magnitudes are distinctly different (Fig. 2). For instance, the rupture nucleated relatively north (blue star in Fig. 2a) within the high locking area ( $>0.75$ ) in the Xue locking model only breaks the updip locked patch, forming an  $M_w$  7.2 earthquake (Fig. 2b). In contrast, the rupture initiated next to it (red star in Fig. 2a) has successfully propagated into the downdip locked patch and ends with an  $M_w$  7.4 earthquake, twice of the moment released by the former one (Fig. 2c). In addition, the slip distribution exhibits appreciable heterogeneity (Fig. 2) in the downdip high locking region ( $>0.75$ ). Such pattern also holds true for the Feng locking model, in which one rupture nearly broke the entire locked patches (Fig. 2e) while the other one nucleating from the neighbouring location did not propagate far from the hypocentre (Fig. 2f), highlighting the dominant effects of heterogeneous stress on rupture propagation.

We then summarize all earthquake magnitudes in our model results. In general, most ruptures initiated in high locking regions (locking degree  $>0.75$ ) will develop into earthquakes with  $M_w \geq 7.2$  in the Nicoya region (Fig. 3). However, ruptures started from the moderate locking region ( $0.5 < \text{locking degree} < 0.75$ ) form smaller earthquakes with  $M_w$  5 to 6. Such trend does not change with the different nucleation sizes (Fig. 3d), although at the same location the earthquake magnitude increases with the nucleation size. One striking feature is that we do not observe any earthquakes with magnitudes between 6 and 7 (Fig. 3d).

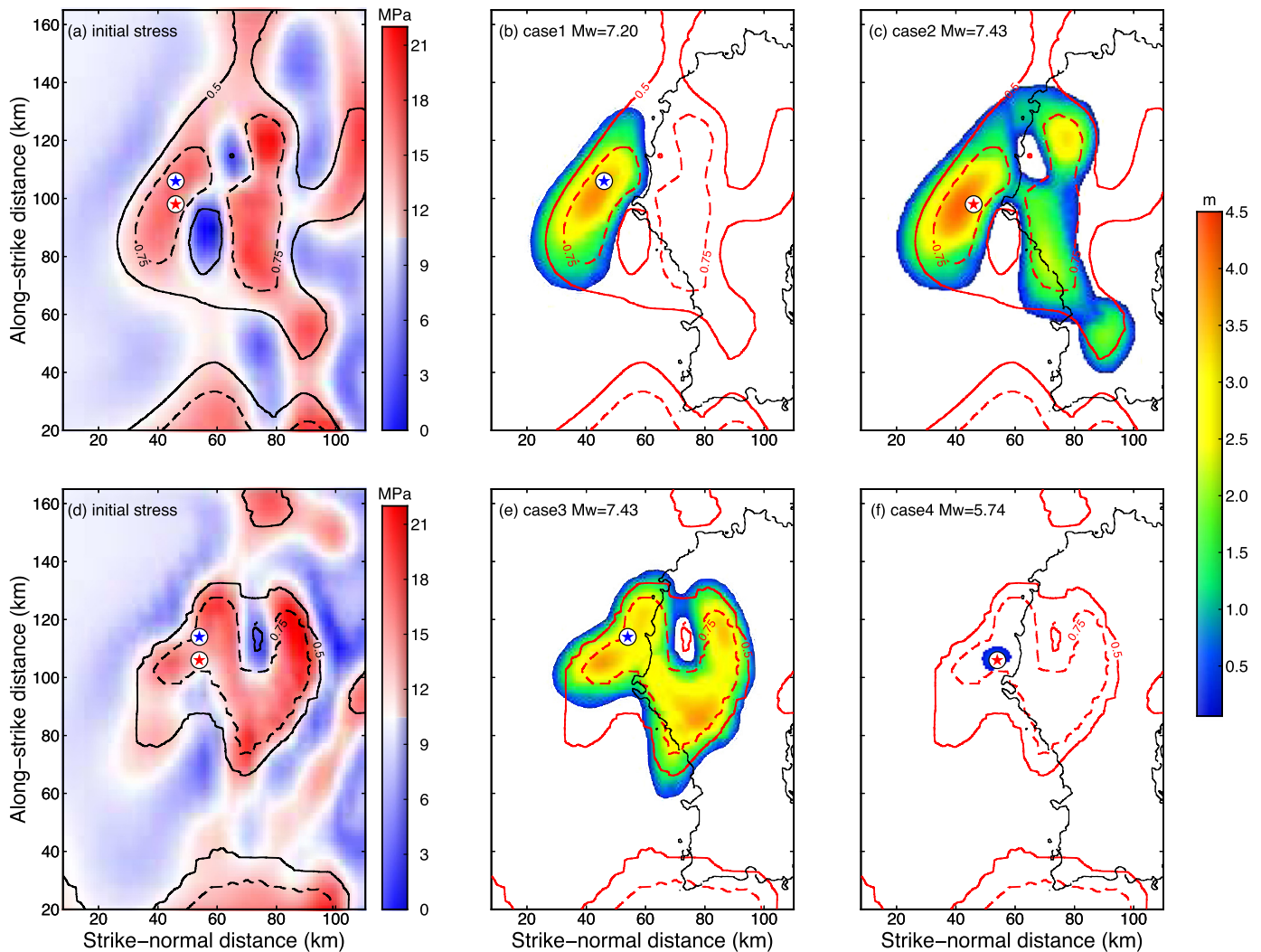


**Fig. 2.** (a) Initial stress distribution that is derived from interseismic locking distribution (Xue et al., 2015). Blue and red stars denote two nucleation zones at the same depth, having identical initial stresses and sizes (5 km). (b) and (c), Slip distribution of scenario earthquakes that were initiated from the blue (b) and red (c) stars. Solid and dashed lines show the locking model. (d), (e), and (f) are same to (a), (b), and (c) panels, respectively, except these are for the Feng locking model (Feng et al., 2012).

We performed the same analysis for the Feng locking model, and found that despite difference in the spatial distribution of locking degrees and the resultant rupture scenarios, the hypocentre-dependent magnitudes are still observed (Fig. 4). In regions with locking degree greater than 0.55, less than 50% of nucleation zones could generate  $M_w > 7$  earthquakes (Fig. 4). Similarly, we do not observe earthquakes with magnitudes of 6 to 7, indicating that the magnitudes of earthquakes are controlled by heterogeneous stress levels on the megathrust if the strength is uniform.

## 4. Discussion

### 4.1. Heterogeneous stress distribution and earthquake magnitude

Although ruptures in this study are artificially initiated, our results are not simply the consequence of nucleation processes. We ensure that stress excess in each nucleation node is identical (i.e. 0.01 MPa) so that the hypocentre dependent earthquake magnitudes are not controlled by the variation in stress excess. It is also shown in our models that nucleating ruptures at regions with nearly identical initial stresses lead to different magnitudes and scenarios (Fig. 2), reflecting the dominant effects on rupture extents of the heterogeneous stress distribution. Indeed, stress field heterogeneity has been shown in a number of studies to signifi-

cantly modulate rupture propagation (e.g., Ripperger et al., 2007; Yang et al., 2012, 2013; Weng et al., 2015).

The hypocentral dependence of magnitudes is a result of the “effective” seismogenic zone induced by the variation in difference between the initial stress and yield strength (uniform in this study) on the fault. As shown in a recent numerical experiment considering finite downdip seismogenic width (Weng and Yang, 2017), ruptures may spontaneously stop without additional structural or stress barriers on a fault with a small seismogenic width. These ruptures are termed self-arresting ruptures, which are caused by the insufficient rupture kinetic energy that is needed to overcome the fracture energy on the fault so that the rupture may continue propagating. In comparison, a fault having a large seismogenic width can host large earthquakes because ruptures can spontaneously propagate and break the entire seismogenic zone (Weng and Yang, 2017), termed breakaway ruptures. In our models, these  $M7+$  earthquake scenarios break at least one highly locked patch because the ruptures started in relatively large “effective” seismogenic region and then propagated much further. Otherwise, they may just form smaller magnitude events (Figs. 3 and 4) due to the limited “effective” seismogenic zone bounded by heterogeneous stress distribution.

In our model, the heterogeneous stress results from the spatial variation in locking where larger gradients lead to higher stress

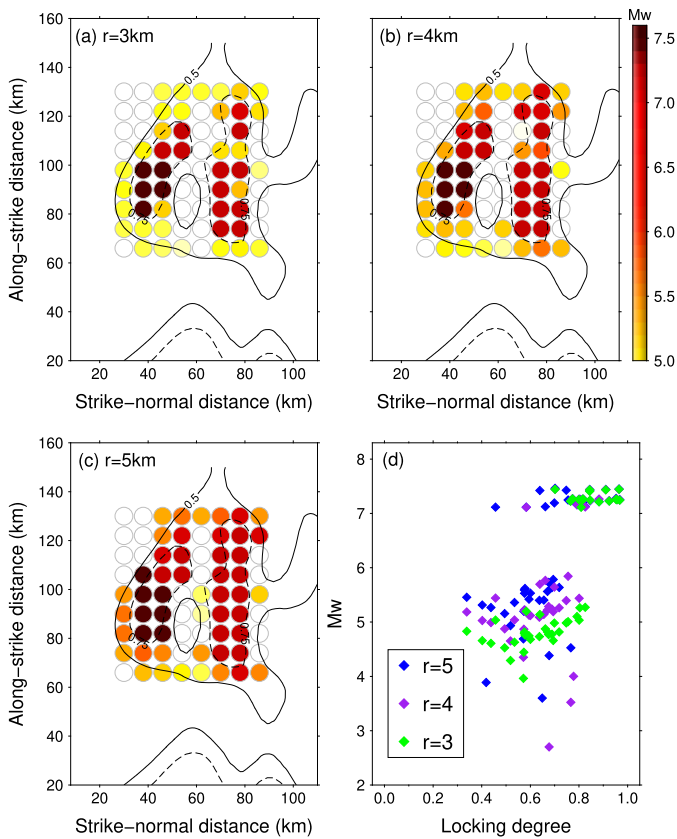


**Fig. 3.** (a), (b), and (c) Map view of the locking degree (contours) and moment magnitudes of rupture scenarios nucleated at each location (circles). Each panel shows the results of different nucleation sizes (3, 4, and 5 km). (d) Relationship between the locking degree and moment magnitudes of location-dependent rupture scenarios, with colours representing different nucleation sizes (3, 4, and 5 km).

(Yin et al., 2016, 2017; Weng and Yang, 2018). In both locking models (Feng et al., 2012; Xue et al., 2015), the grid size on the megathrust is 5 km and the resolution is more than 20 km so that strong variations in a small spatial scale may not be captured. Again, the same caveat about considering only the relative nature of these results is because they are derived from subjectively smoothed locking models. The faults are likely much more heterogeneous, forming smaller asperities that cannot be easily observed with surface geodetic techniques. If such small asperities rupture, we should then observe a large number of moderate interface earthquakes, which is however not the case in the Nicoya region (Fig. 1). From 1976 to September 2012, we only find 7 earthquakes with  $M_w$  5+ from the GCMT catalogue that had thrust mechanisms (Fig. 1). Five out of the seven events are located in the locking region, while others are outside (Fig. 1a). For  $\sim 82$  mm/yr of convergence (DeMets et al., 2010), the lack of more frequent moderate earthquakes implies strong locking with limited small-scale heterogeneities, which were perhaps caused by seafloor roughness as is immediately to the south (Bilek et al., 2003). The magnitude gap (M6–7) in our numerical results, irrespective of the input locking models, is consistent with observations beneath Nicoya prior to the 2012 mainshock, in which earthquakes with magnitudes between 5.5 and 7 are very rare (Fig. 1c). Even if we consider the time window after the mainshock, the magnitudes of most aftershocks do not exceed 5.5 (Chaves et al., 2017). Thus the magnitude gap may reflect to some extents the spatial heterogeneity of stress and locking in the Nicoya region.

In contrast, there are a number of shallow thrust earthquakes with magnitudes 5–6+ in the region northwest to the locked patches (Fig. 1), indicating abundant small asperities. High-

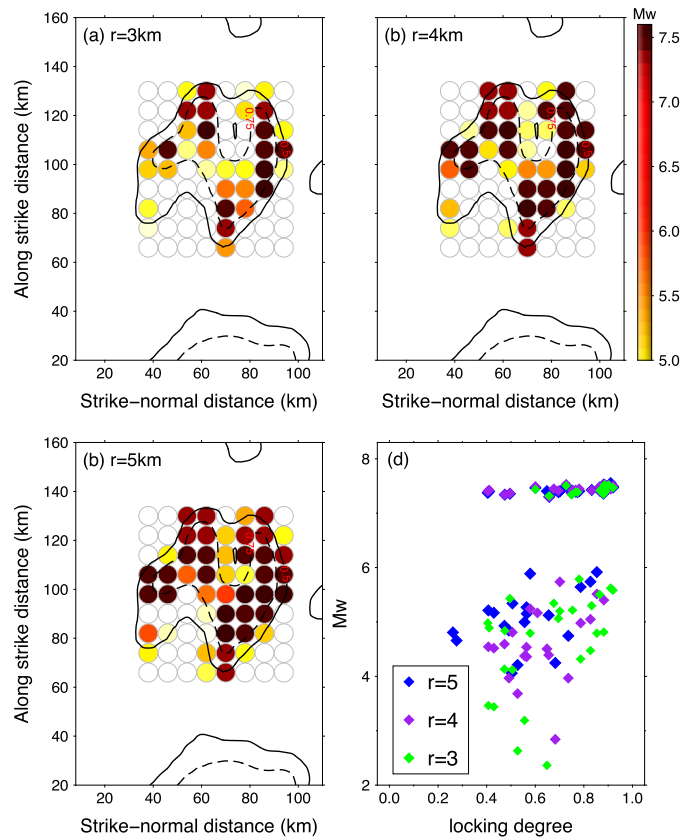


**Fig. 4.** Same with Fig. 3, except for the Feng locking model.

resolution locking models based on geodetic data are not available due to the lack of constraint on the shallow megathrust. But this portion is likely creeping, and the creeping is associated with numerous normal faulting fabrics and potentially subducted seamounts (Wang and Bilek, 2014).

#### 4.2. Implications on earthquake and tsunami hazard assessment

In addition to estimating the locations and sizes of potential earthquakes, practical seismic assessments should also forecast local ground shaking to evaluate hazard and mitigate risk. Our results show that, although two earthquake scenarios initiating from high locking regions may have the same magnitude in the Nicoya Peninsula, the ground motion could be drastically different due to rupture directivity. To exemplify this, we nucleated two earthquakes with similar magnitudes (i.e. 7.42 and 7.49) from the Feng locking model, while one initiated from offshore and the other one nucleated inland (Fig. 5). For the two cases, the ruptures break both offshore and beneath land, resulting in similar final slip distribution (Fig. 5a and b). When the rupture initiated from inland (Fig. 5b), the up-dip propagating rupture would lead to much higher ground velocity offshore, as shown in the record of a hypothetical station at P1 (Fig. 5f); while the down-dip rupture will produce nearly as twice as large of peak-to-peak vertical velocity at the town of Nicoya (Fig. 5d), despite that the town is much closer to the epicentre of up-dip case rupture (Fig. 5b).

In addition to playing roles in ground shaking, the rupture directivity affects shallow slip distribution and potential tsunami generation. For the rupture nucleated offshore (Fig. 5a), the peak ground displacements along a profile (i.e. along-strike distance equals to 105 km) show uplift of the ruptured area, with the maximum displacement of  $\sim 0.9$  m near the epicentre (Fig. 5c). In contrast, the rupture nucleated from below land, and propagating

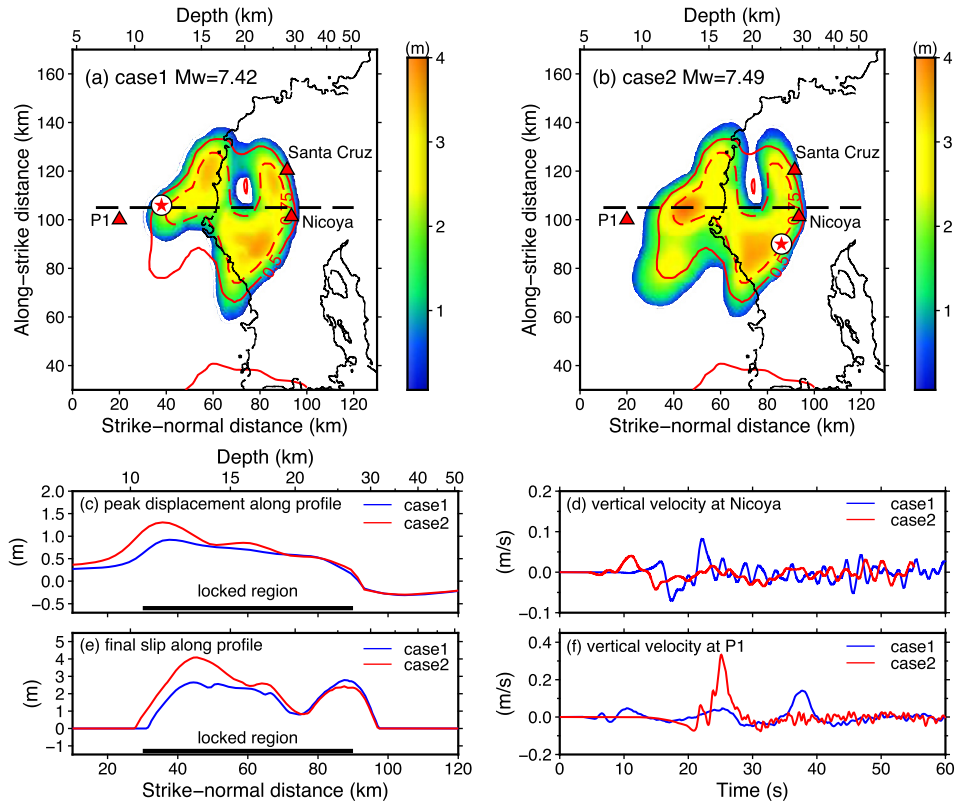


**Fig. 5.** Final slip distribution of rupture scenarios nucleated at two different locations, offshore (a) and inland (b), using the Feng locking model (contours) with nucleation sizes of 4 km. Dash lines show a profile to compare ground displacements. Triangles denote hypothetical stations, one offshore (P1) and two at towns of Nicoya and Santa Cruz. Peak displacements (c) and final slip distribution (e) along the profile from the two rupture scenarios. Vertical velocities recorded at Nicoya (d) and P1 (f) from the two scenarios, respectively.

up-dip, would lead to larger shallow slip (Fig. 5e) and ground displacements (Fig. 5c) along the profile than in the prior scenario, due to the rupture directivity. In the offshore region, the ground displacement could be amplified nearly twice (Fig. 5c), and such up-dip environment is more prone to tsunami excitation.

We then summarize the slip distributions for all rupture scenarios nucleating from different hypocentres that have nearly identical moment magnitudes ( $>7.4$ ). For ruptures initiating from shallow depths (i.e.  $<18$  km) in the Nicoya region (Fig. 6a), the downdip slip amplitudes are similar with those nucleating from greater depths (Fig. 6b). In addition, the amplitudes and depths of peak slip show quite good consistency in the deeper part with those during the 2012 Nicoya earthquake, which nucleated from offshore (Yue et al., 2013). In contrast, the slip at shallow depths ( $<15$  km) resulting from deeper hypocentres are obviously larger than those nucleating at shallow depths (Fig. 6b). Such systematically larger shallow slips from deeper nucleation points will lead to larger ground displacements offshore, which in turn increase the tsunamic-genetic potential.

Interestingly, the  $M_w$  7.7 1950 Nicoya earthquake, while centred similarly below the peninsula, did create a meter-level tsunami across portions of the southern peninsula, and up to 10 cm inside the Gulf of Nicoya, despite having 12 yr less to rebuild since its last major event in 1900 (Protti, 2001). Perhaps the major difference between the 1950 and 2012 events are not the prior locking, but where nucleation initiated, the 1950 event initiating down-dip (Guendel, 1986), and the 2012 earthquake initiating up-dip (Yue et al., 2013).

Megathrust earthquakes may generate tsunami by causing significant vertical seafloor displacement or less commonly by generating submarine landslides. As shown above, based on Feng’s locking model, the rupture that nucleated from the high-locking

region generated substantially larger ground displacements on the seafloor due to up-dip rupture directivity (Fig. 5), and may lead to tsunami generation. If we can produce a large number of ground motion database for each rupture scenario at different hypocentres with a reliable locking model, then the seafloor ground movements can lead to tsunami wave height prediction along the coast by conducting numerical simulation of tsunami waves, given appropriate bathymetric information. In the most optimistic case, an earthquake hypocentre can be automatically determined with high-resolution by local seismic network, and can then be directly used to predict potential tsunami wave heights from the pre-computed database from one of the determined scenario runs. A more realistic approach would be to include a probability-distribution function of scenario inundations for a given hypocentre and an estimation of error in its location. Because tsunami waves propagate much slower than seismic waves, such approach would be effective for near-field earthquake-induced tsunami early-warning.

**5. Conclusions**

In this study, we quantitatively evaluate potential earthquake sizes and rupture scenarios from interseismic locking models and demonstrate that the initiation point of the rupture plays critical roles in controlling the earthquake sizes due to the heterogeneous stress distribution. Our results show that ruptures initiating from high locking zones more likely grow into larger earthquakes, with 40% becoming  $M > 7.2$  in Nicoya Peninsula. Irrespective of the input locking models we do not find scenario ruptures that have magnitudes of 6–7, which is largely consistent with observations and probably reflects to some extents the degree of stress heterogeneity in the Nicoya Peninsula. Furthermore, the rupture directivity effects are critical in ground shaking and displacement

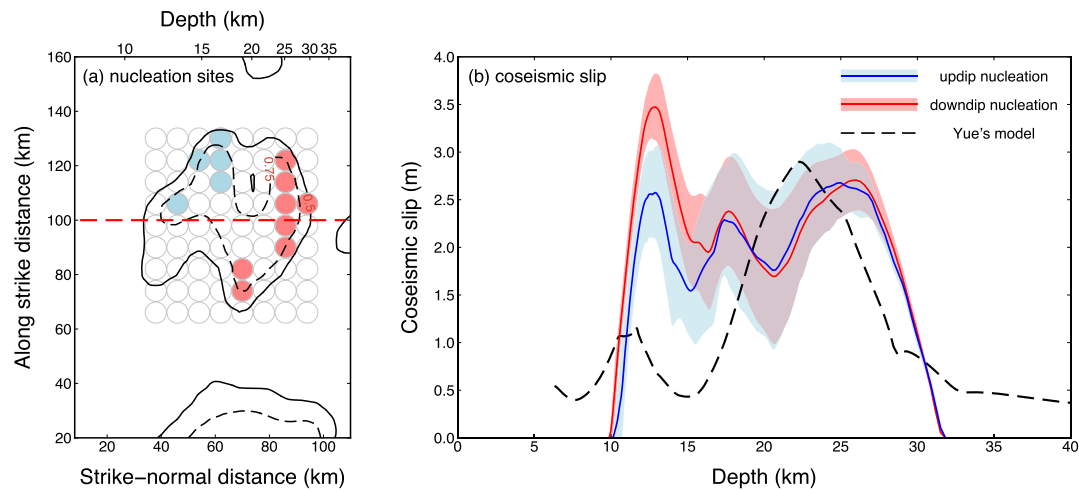


**Fig. 6.** (a) Updip (light blue) and downdip (red) nucleation locations with nearly identical final moment magnitudes ( $M_w > 7.4$ ) of rupture scenarios. Contours show the locking distribution. (b) Slip distributions from all rupture scenarios along a profile (red dash line) shown in panel (a). Red and blue lines show the average values, and the shaded areas indicate the 1- $\sigma$  confidence. Black dashed line is from Yue's kinematic source model (Yue et al., 2013).

prediction given the same earthquake magnitude, shedding lights on near-field tsunami early warning. The results of hypocentre-dependent earthquake magnitudes in a given interseismic locking distribution pose challenges, yet the numerically derived rupture scenarios can be used for evaluating earthquake and tsunami hazard.

#### Data availability

All results in this study are generated from numerical simulations and can be requested by contacting the corresponding author.

#### Acknowledgements

The authors thank support from Hong Kong Research Grant Council Grants (24601515, 14313816, 14306418), Direct Grant from Faculty of Science at the Chinese University of Hong Kong, China Earthquake Science Experiment Project, CEA (grant No. 2017CESE0103), and State Key Lab of Earthquake Dynamics (grant No. LED2017B07), Institute of Geology, CEA. The authors also appreciate constructive comments from two anonymous reviewers.

#### Appendix A. Supplementary material

Supplementary material related to this article can be found online at <https://doi.org/10.1016/j.epsl.2019.05.030>.

#### References

Aagaard, B.T., Knepley, M.G., Williams, C.A., 2013. A domain decomposition approach to implementing fault slip in finite-element models of quasi-static and dynamic crustal deformation. *J. Geophys. Res.* 118, 3059–3079.

Audet, P., Schwartz, S.Y., 2013. Hydrologic control of forearc strength and seismicity in the Costa Rican subduction zone. *Nat. Geosci.* 6 (10), 852–855.

Bilek, S.L., Schwartz, S.Y., DeShon, H.R., 2003. Control of seafloor roughness on earthquake rupture behavior. *Geology* 31 (5), 455–458. [https://doi.org/10.1130/0091-7613\(2003\)031](https://doi.org/10.1130/0091-7613(2003)031).

Bizzarri, A., 2010. How to promote earthquake ruptures: different nucleation strategies in a dynamic model with slip-weakening friction. *Bull. Seismol. Soc. Am.* 100, 923–940.

Burgette, R.J., Weldon, R.J., Schmidt, D.A., 2009. Interseismic uplift rates for western Oregon and along-strike variation in locking on the Cascadia subduction zone. *J. Geophys. Res.* 114, B01408.

Chaves, E.J., Schwartz, S.Y., 2016. Monitoring transient changes within overpressured regions of subduction zones using ambient seismic noise. *Sci. Adv.* 2, e1501289.

Chaves, E.J., Duboeuf, L., Schwartz, S.Y., Lay, T., Kintner, J., 2017. Aftershocks of the 2012 Mw 7.6 Nicoya, Costa Rica, earthquake and mechanics of the plate interface. *Bull. Seismol. Soc. Am.* 107 (3), 1227–1239. <https://doi.org/10.1785/0120160283>.

DeMets, C., Gordon, R.G., Argus, D.F., 2010. Geologically current plate motions. *Geophys. J. Int.* 181 (1), 1–80.

Dixon, T.H., Jiang, Y., Malservisi, R., McCaffrey, R., Voss, N., Protti, M., Gonzalez, V., 2014. Earthquake and tsunami forecasts: relation of slow slip events to subsequent earthquake rupture. *Proc. Natl. Acad. Sci. USA* 111 (48), 17039–17044.

Feng, L., Newman, A.V., Protti, M., Gonzalez, V., Jiang, Y., Dixon, T.H., 2012. Active deformation near the Nicoya Peninsula, northwestern Costa Rica, between 1996 and 2010: interseismic megathrust coupling. *J. Geophys. Res., Solid Earth* 117, B06407.

Guendel, F., 1986. Seismotectonics of Costa Rica: An Analytical View of the Southern Terminus of the Middle America Trench. Ph.D. Thesis, Univ. of Calif., Santa Cruz. 157 pp.

Hok, S., Fukuyama, E., Hashimoto, C., 2011. Dynamic rupture scenarios of anticipated Nankai-Tonankai earthquakes, southwest Japan. *J. Geophys. Res.* 116, B12319.

Hori, T., Kato, N., Hirahara, K., Baba, T., Kaneda, Y., 2004. A numerical simulation of earthquake cycles along the Nankai Trough in southwest Japan: lateral variation in frictional property due to the slab geometry controls the nucleation position. *Earth Planet. Sci. Lett.* 228 (3), 215–226.

Ida, Y., 1972. Cohesive force across the tip of a longitudinal-shear crack and Griffith's specific surface energy. *J. Geophys. Res.* 77 (20), 3796–3805.

Kyriakopoulos, C., Newman, A.V., 2016. Structural asperity focusing locking and earthquake slip along the Nicoya megathrust, Costa Rica. *J. Geophys. Res., Solid Earth* 121 (7), 5461–5476.

Kyriakopoulos, C., Newman, A.V., Thomas, A.M., Moore-Driskell, M., Farmer, G.T., 2015. A new seismically constrained subduction interface model for Central America. *J. Geophys. Res.* 120 (8), 5535–5548.

Lapusta, N., Rice, J.R., 2003. Nucleation and early seismic propagation of small and large events in a crustal earthquake model. *J. Geophys. Res., Solid Earth* 108 (B4), B000793.

Li, S., Wang, K., Wang, Y., Jiang, Y., Dosso, S.E., 2018. Geodetically inferred locking state of the Cascadia megathrust based on a viscoelastic Earth model. *J. Geophys. Res., Solid Earth* 123. <https://doi.org/10.1029/2018JB015620>.

McCaffrey, R., King, R.W., Payne, S.J., Lancaster, M., 2013. Active tectonics of northwestern US inferred from GPS-derived surface velocities. *J. Geophys. Res., Solid Earth* 118 (2), 709–723.

Moreno, M., Rosenau, M., Oncken, O., 2010. 2010 Maule earthquake slip correlates with pre-seismic locking of Andean subduction zone. *Nature* 467 (7312), 198–202.

Pollitz, F.F., Evans, E.L., 2017. Implications of the earthquake cycle for inferring fault locking on the Cascadia megathrust. *Geophys. J. Int.* 209, 167–185. <https://doi.org/10.1093/gji/ggx009>.

Protti, M., 2001. Significance of an earthquake early warning system for vulnerable essential facilities: the example of a potential implementation in Costa Rica. *ISDR Inf.* 3, 21–4.

Quintero, R., Zahradník, J., Sokos, E., 2014. Near-regional CMT and multiple-point source solution of the September 5, 2012, Nicoya, Costa Rica Mw 7.6 (GCMT) earthquake. *J. South Am. Earth Sci.* 55, 155–165.

Rice, J.R., 1992. Fault stress state, pore pressure distributions, and the weakness of San Andreas Fault. In: *Fault Mechanics and Transport Properties of Rocks*. Academic Press, San Diego, CA, pp. 475–503.

Ripperger, J., Ampuero, J.-P., Mai, P.M., Giardini, D., 2007. Earthquake source characteristics from dynamic rupture with constrained stochastic fault stress. *J. Geophys. Res.* 112, B04311.

Saffer, D.M., Tobin, H.J., 2011. Hydrogeology and mechanics of subduction forearcs: fluid flow and pore pressure. *Annu. Rev. Earth Planet. Sci.* 39 (1), 157–186.

- Schmalzle, G.M., McCaffrey, R., Creager, K.C., 2014. Central Cascadia subduction zone creep. *Geochem. Geophys. Geosyst.* 15, 1515–1532. <https://doi.org/10.1002/2013GC005172>.
- Wang, K., Bilek, S.L., 2014. Fault creep caused by subduction of rough seafloor relief. *Tectonophysics* 610, 1–24.
- Wang, K., Hu, Y., He, J., 2012. Deformation cycles of subduction earthquakes in a viscoelastic Earth. *Nature* 484 (7394), 327–332.
- Weng, H., Yang, H., 2017. Seismogenic width controls aspect ratios of earthquake ruptures. *Geophys. Res. Lett.* 44 (6), 2725–2732.
- Weng, H., Yang, H., 2018. Constraining frictional properties on fault by dynamic rupture simulations and near-field observations. *J. Geophys. Res.* <https://doi.org/10.1029/2017JB015414>.
- Weng, H., Huang, J., Yang, H., 2015. Barrier-induced supershear ruptures on a slip-weakening fault. *Geophys. Res. Lett.* 42 (12), 4824–4832.
- Williamson, A.L., Newman, A.V., 2018. Limitations of the resolvability of finite-fault models using static land-based geodesy and open-ocean tsunami waveforms. *J. Geophys. Res.* 123. <https://doi.org/10.1029/2018JB016091>.
- Xue, L., Schwartz, S., Liu, Z., Feng, L., 2015. Interseismic megathrust coupling beneath Nicoya Peninsula, Costa Rica, from the joint inversion of InSAR and GPS data. *J. Geophys. Res.* 120 (5), 3707–3722.
- Yang, H., Liu, Y., Lin, J., 2012. Effects of subducted seamount on megathrust earthquake nucleation and rupture propagation. *Geophys. Res. Lett.* 39, L24302.
- Yang, H., Liu, Y., Lin, J., 2013. Geometrical effects of a subduction seamount on stopping megathrust rupture. *Geophys. Res. Lett.* 40 (10), 2011–2016.
- Yang, H., Yao, S., He, B., Newman, A., Weng, H., 2019. Deriving rupture scenarios from interseismic locking distributions along the subduction megathrust. *J. Geophys. Res.*, in preparation.
- Yao, S., Yang, H., 2018. Determination of coseismic frictional properties on the megathrust during the 2012 M7.6 Nicoya earthquake. In: AGU Fall Meeting, T41H-0407.
- Yin, J., Yang, H., Yao, H., Weng, H., 2016. Coseismic radiation and stress drop during the 2015 Mw 8.3 Illapel, Chile megathrust earthquake. *Geophys. Res. Lett.* 43, 1520–1528.
- Yin, J., Yao, H., Yang, H., Liu, J., Qin, W., Zhang, H., 2017. Frequency-dependent rupture process, stress change, and seismogenic mechanism of the 25 April 2015 Nepal Gorkha Mw 7.8 earthquake. *Sci. China Earth Sci.* 60 (4), 796–808.
- Yue, H., Lay, T., Schwartz, S.Y., Rivera, L., Protti, M., Dixon, T.H., Owen, S., Newman, A.V., 2013. The 5 September 2012 Nicoya, Costa Rica Mw 7.6 earthquake rupture process from joint inversion of high-rate GPS, strong-motion, and teleseismic P wave data and its relationship to adjacent plate boundary interface properties. *J. Geophys. Res., Solid Earth* 118 (10), 5453–5466.